

# Applications of the optical fiber to the generation and measurement of low-phase-noise microwave signals

Kirill Volyanskiy,<sup>1,2</sup> Johann Cussey,<sup>1,3</sup> Hervé Tavernier,<sup>1</sup> Patrice Salzenstein,<sup>1</sup> Gérard Sauvage,<sup>4</sup> Laurent Larger,<sup>1</sup> and Enrico Rubiola<sup>1,\*</sup>

<sup>1</sup>Franche Comté Electronique, Mécanique, Thermique, Optique - Sciences and Technologies (FEMTO-ST) Institute, CNRS and Université de Franche Comté, Besançon, France

<sup>2</sup>St. Petersburg State University of Aerospace Instrumentation, Russia

<sup>3</sup>Smart Quantum, Lannion and Besançon, France

<sup>4</sup>Aeroflex, Elancourt (Paris), France

\*Corresponding author: rubiola@femto-st.fr

Received July 29, 2008; revised September 23, 2008; accepted September 30, 2008; posted October 6, 2008 (Doc. ID 99499); published November 26, 2008

The optical fiber used as a microwave delay line exhibits high stability and low noise and makes accessible a long delay ( $\geq 100 \mu\text{s}$ ) in a wide bandwidth ( $\approx 40 \text{ GHz}$ , limited by the optronic components). Hence, it finds applications as the frequency reference in microwave oscillators and as the reference discriminator for the measurement of phase noise. The fiber is suitable to measure the oscillator stability with a sensitivity of parts in  $10^{-12}$ . Enhanced sensitivity is obtained with two independent delay lines, after correlating and averaging. Short-term stability of parts in  $10^{-12}$  is achieved inserting the delay line in an oscillator. The frequency can be set in steps multiple of the inverse delay, which is in the 10–100 kHz region. We add to the available references a considerable amount of engineering and practical knowledge, the understanding of  $1/f$  noise, calibration, the analysis of the cross-spectrum technique to reduce the instrument background, the phase-noise model of the oscillator, and the experimental test of the oscillator model. © 2008 Optical Society of America

OCIS codes: 000.3110, 060.5625, 120.3940, 120.5050, 350.4010.

## 1. INTRODUCTION

Science and technology require reference microwave sources with ever increasing stability and spectral purity, and, of course, suitable measurement systems. The frequency synthesis from the HF/VHF region is no longer satisfactory because of the insufficient spectral purity inherent in the multiplication and because of more trivial limitations such as mass, volume, and complexity. The domain of RF–microwave photonics is growing fast [1]. The generation of microwaves from optics, or more generally “with optics,” is providing new solutions. Examples are mode-locked lasers [2,3], optoelectronic oscillators (OEOs) [4,5], optical microcavities [6], optical parametric oscillators (OPOs) [7,8], and frequency combs [9].

The optical fiber used as a delay line enables the generation [4,5] and the measurement [10] of stable and highly spectrally pure microwave signals. The optical fiber is a good choice for the following reasons.

1. A long delay can be achieved, of 100  $\mu\text{s}$  and more, thanks to the low loss (0.2 dB/km at 1.55  $\mu\text{m}$  and 0.35 dB/km at 1.31  $\mu\text{m}$ ).
2. The frequency range is wide, at least of 40 GHz, still limited by the optoelectronic components
3. The background noise is low, close to the limit imposed by the shot noise and by the thermal noise at the detector output.
4. The thermal sensitivity of the delay ( $6.85 \times 10^{-6}/\text{K}$ )

is a factor of 10 lower than the sapphire dielectric cavity at room temperature. This resonator is considered the best ultrastable microwave reference.

5. In oscillators and phase-noise measurements the microwave frequency is the inverse of the delay. This means that the oscillator or the instrument can be tuned in steps of  $10^{-5}$ – $10^{-6}$  of the carrier frequency without degrading stability and spectral purity with frequency synthesis. Finer-tuning is possible at a minimum cost in terms of stability and spectral purity.

We describe a series of experiments related to the generation and measurement of low-phase-noise microwave signals using a delay implemented with an intensity-modulated beam propagating through an optical fiber. A 10 GHz oscillator prototype exhibits a frequency flicker of  $3.7 \times 10^{-12}$  (Allan deviation) and a phase noise lower than  $-140 \text{ dBrad}^2/\text{Hz}$  at 10 kHz off the carrier. The same values are achieved as the sensitivity in phase noise measurements in real time. This sensitivity is sufficient to measure the frequency flicker of a sapphire oscillator, which is considered the reference in the field of low-noise microwave oscillators [11]. In phase-noise measurements enhanced sensitivity is obtained with the cross-spectrum method, which takes correlation and averaging on two independent delay lines.

This paper stands on [4] for the oscillator and on [10,12] for the measurements. We aim at providing prac-

tical knowledge, adding engineering, accurate calibration, the analysis of the cross-spectrum technique, the phase-noise model of the oscillator, and experimental tests.

## 2. BASIC CONCEPTS

### A. Phase Noise

Phase noise is a well-established subject, clearly explained in classical references, among which we prefer [13–16] and [[17], Vol. 1, Chap. 2]. The quasi-perfect sinusoidal signal of frequency  $\nu_0$ , of random amplitude fluctuation  $\alpha(t)$ , and of random phase fluctuation  $\varphi(t)$  is

$$v(t) = [1 + \alpha(t)]\cos[2\pi\nu_0 t + \varphi(t)]. \quad (1)$$

We may require that  $|\alpha(t)| \ll 1$  and  $|\varphi(t)| \ll 1$  during the measurement. The phase noise is generally measured as the average power spectral density (PSD)

$$S_\varphi(f) = \langle |\Phi(jf)|^2 \rangle_m \quad (\text{average, } m \text{ spectra}), \quad (2)$$

where the uppercase denotes the Fourier transform, so  $\varphi(t) \leftrightarrow \Phi(jf)$  form a transform inverse-transform pair. In experimental science the single-sided PSD is preferred to the two-sided PSD because the negative frequencies are redundant. It has been found that the power-law model describes accurately the phase noise of the oscillator and components

$$S_\varphi(f) = \sum_{n=-4}^0 b_n f^n \quad (\text{power law}), \quad (3)$$

Coefficient	Noise Type
$b_{-4}$	Frequency random walk
$b_{-3}$	Flicker of frequency
$b_{-2}$	White frequency noise, or phase random walk
$b_{-1}$	Flicker of phase
$b_0$	White phase noise

The power law relies on the fact that white ( $f^0$ ) and flicker ( $1/f$ ) noises exist per se, and that a phase integration is present in oscillators, which multiplies the spectrum by  $1/f^2$ . If needed, the model can be extended to  $n < -4$ . Of course, the power law can also be used to describe the spectrum of the fractional frequency fluctuation  $y(t) = \dot{\varphi}(t)/2\pi\nu_0$ ,

$$S_y(f) = \frac{f^2}{\nu_0^2} S_\varphi(f) = \sum_{n=-2}^2 h_n f^n. \quad (4)$$

Another tool often used is the two-sample (Allan) variance  $\sigma_y^2(\tau)$  as a function of the measurement time  $\tau$ . Notice that the symbol  $\tau$  is commonly used for the measurement time and for delay of the line (Subsection 2.C). We will add a subscript when needed. For the most useful frequency-noise processes, the relation between  $\sigma_y^2(\tau)$  and  $S_y(f)$  is

$$\sigma_y^2(\tau) = \begin{cases} \frac{h_0}{2\tau} & \text{white frequency noise} \\ h_{-1} 2 \ln(2) & \text{flicker of frequency.} \\ h_{-2} \frac{(2\pi)^2}{6} \tau & \text{frequency random walk} \end{cases} \quad (5)$$

### B. Cross-Spectrum Method

Inevitably, the measured noise is the sum of the device-under-test (DUT) noise and of the the instrument background. Improved sensitivity is obtained with a correlation instrument, in which two separate channels measure simultaneously the same DUT. Let  $a(t) \leftrightarrow A(jf)$  and  $b(t) \leftrightarrow B(jf)$  be the backgrounds of the two instruments, and  $c(t) \leftrightarrow C(jf)$  be the DUT noise or any common noise. The two instrument outputs are

$$x(t) = c(t) + a(t), \quad (6)$$

$$y(t) = c(t) + b(t), \quad (7)$$

where  $a(t)$ ,  $b(t)$ , and  $c(t)$  are statistically independent because we have put all the common noise in  $c(t)$ . The cross-spectrum averaged on  $m$  measures is

$$\begin{aligned} S_{yx}(f) &= \langle YX^* \rangle_m = \langle CC^* \rangle_m + \langle CB^* \rangle_m + \langle AC^* \rangle_m + \langle AB^* \rangle_m \\ &= S_c(f) + O(\sqrt{1/m}), \end{aligned} \quad (8)$$

where  $O(\cdot)$  means “order of.” Owing to the statistical independence of  $a(t)$ ,  $b(t)$ , and  $c(t)$ ,  $A(jf)$ ,  $B(jf)$ , and  $C(jf)$  are also statistically independent. Hence, the cross terms decrease as  $\sqrt{1/m}$ . This enables one to interpret  $S_{yx}(f)$  as follows.

**Statistical limit.** With no DUT noise and with two fully independent channels, it holds that  $c(t) = 0$ . After Eq. (8) the statistical limit of the measurement is

$$S_{yx}(f) \approx \sqrt{\frac{1}{m} S_a(f) S_b(f)} \quad (\text{statistical limit}). \quad (9)$$

Accordingly, a 5 dB improvement on the single-channel noise costs a factor of 10 in averaging, thus in measurement time.

**Correlated hardware background.** Still at zero DUT noise, we break the hypothesis of statistical independence of the two channels. We interpret  $c(t)$  as the correlated noise of the instrument, due to environment, to the cross talk between the two channels, etc. This is the hardware limit of the instrument sensitivity

$$S_{yx}(f) \approx [S_c(f)]_{\text{xtalk, etc.}} \quad (\text{hardware limit}). \quad (10)$$

**Regular DUT measurement.** Now we introduce the DUT noise. Under the assumptions that

1.  $m$  is large enough for the statistical limit to be negligible, and

2. The correlated background is negligible as compared to the DUT noise, the cross spectrum gives the DUT noise

$$S_{yx}(f) \approx [S_c(f)]_{\text{DUT}} \quad (\text{DUT measurement}). \quad (11)$$

This is the regular use of the instrument.

### C. Delay Line Theory

Delaying the signal  $v(t)$  by  $\tau$ , all time-varying parameters of  $v(t)$  are also delayed by  $\tau$ , thus the phase fluctuation  $\varphi(t)$  turns into  $\varphi(t - \tau)$ . By virtue of the time-shift theorem, the Fourier transform of  $\varphi(t - \tau)$  is  $e^{-j2\pi\tau f}\Phi(jf)$ . This enables the measurement of the oscillator phase noise  $\varphi(t)$  by observing the difference  $\theta(t) = \varphi(t) - \varphi(t - \tau)$ . Referring to Fig. 1, the output signal is  $V_o(jf) = k_\varphi \Theta(jf) = k_\varphi H(jf)\Phi(jf)$ , where  $k_\varphi$  is the mixer phase-to-voltage gain, and  $H(jf) = 1 - e^{-j2\pi\tau f}$  is the system transfer function. Consequently

$$S_v(f) = k_\varphi^2 |H(jf)|^2 S_\varphi(f), \tag{12}$$

$$|H(jf)|^2 = 4 \sin^2(\pi f \tau). \tag{13}$$

The oscillator noise  $S_\varphi(f)$  is inferred by inverting Eq. (12). In practice, it is important to keep  $S_v(f)$  accessible because it reveals most of the experimental mistakes connected with the instrument background. The function  $|H(jf)|^2$  has a series of zeros at  $f = n/\tau$ , integer  $n$ , in the vicinity of which the experimental results are not useful. In fact, inverting Eq. (12) yields a series of sharp peaks at  $f = n/\tau$  generated by the division by zero, which of course do not exist in the oscillator spectrum. This will be seen, for example, in Fig. 6, where the use of 4 km fiber ( $\tau = 20 \mu\text{s}$ , curve f, black) gives peaks at 50 and 100 kHz (the latter only partially visible because of the 100 kHz span), while the spectrum measured at the mixer output (curve a, red) to be plugged in Eq. (12) is smooth. This figure will be discussed in Subsection 5.A. Additional care must be spent in the measurement of a delay-line oscillator, which has its own noise peaks for the reasons detailed in Subsection 2.D. In practice, the first zero of  $|H(jf)|^2$  sets the maximum measurement bandwidth to  $0.95/\tau$ , as discussed in [10]. Nonetheless, the regions between contiguous zeros are useful diagnostics for the oscillator under test, provided that the frequency resolution of the fast Fourier transform (FFT) analyzer be sufficient.

At low frequency the instrument background is naturally optimized for the measurement of  $1/f^2$  and  $1/f^3$  noise because  $1/|H(jf)|^2 \sim 1/f^2$  for  $f \rightarrow 0$ , and an additional factor  $1/f$  comes from the electronics. This is a fortunate outcome because the noise of the oscillators of major interest is proportional to  $1/f^3$  or to  $1/f^4$  in this region. Of course, an appropriate choice of  $\tau$  is necessary.

### D. Oscillator Phase Noise

The oscillator consists of an amplifier of gain  $A$  (assumed constant versus frequency) and a feedback transfer function  $\beta(jf)$  in a closed loop. The gain  $A$  compensates for the losses, while  $\beta(jf)$  selects the oscillation frequency. This model is general, independent of the nature of  $A$  and  $\beta(jf)$ . We assume that the Barkhausen condition  $|A\beta(jf)| = 1$  for

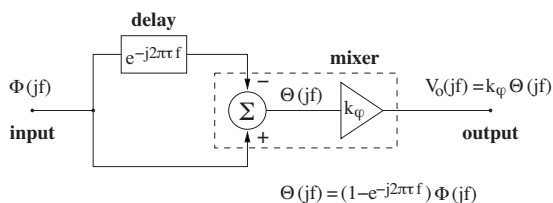


Fig. 1. Basic delay-line phase noise measurement.

stationary oscillation is verified at the carrier frequency  $\nu_0$  by saturation in the amplifier or by some other gain-control mechanism. Under this hypothesis, the phase noise is modeled by the scheme of Fig. 2, where all signals are the phases of the oscillator loop [18,19]. This model is inherently linear, so it eliminates the mathematical difficulty due to the parametric nature of flicker noise and of the noise originated from the environment fluctuations. We denote with  $\varphi(t) \leftrightarrow \Phi(jf)$  the oscillator phase noise, and with  $\psi(t) \leftrightarrow \Psi(jf)$  the amplifier phase noise. The latter is always additive, regardless of the underlying physical mechanism. More generally,  $\psi(t)$  accounts for the phase noise of all the electronic and optical components in the loop. The ideal amplifier “repeats” the phase of the input, for it has a gain of 1 (exact) in the phase-noise model. The feedback path is described by the transfer function  $B(jf)$  of the phase perturbation. In the case of the delay-line oscillator, the feedback path is a delay line of delay  $\tau_d$  followed by a resonator of relaxation time  $\tau_f \ll \tau_d$  that selects the oscillation frequency  $\nu_0$  among the multiples of  $1/\tau_d$ . Neglecting the difference between the natural and oscillation frequencies,  $\tau_f$  is related to the quality factor  $Q$  by  $\tau_f = Q/\pi\nu_0$ . The phase-perturbation response of the feedback path is

$$B(jf) = \frac{e^{-j2\pi f \tau_d}}{1 + j2\pi f \tau_f}. \tag{14}$$

The oscillator is described by the phase-noise transfer function

$$H(jf) = \frac{\Phi(jf)}{\Psi(jf)} \quad [\text{definition of } H(jf)]. \tag{15}$$

Using the basic equations of feedback, by inspection of Fig. 2 we find

$$H(jf) = \frac{1}{1 - B(jf)}, \tag{16}$$

and consequently

$$|H(jf)|^2 = \frac{1 + 4\pi^2 f^2 \tau_f^2}{2 - 2 \cos(2\pi f \tau_d) + 4\pi^2 f^2 \tau_f^2 + 2\omega \tau_f \sin(2\pi f \tau_d)}. \tag{17}$$

The detailed proof of Eqs. (14) and (17) is given in [18,19]. The result is confirmed using the phase diffusion and the formalism of stochastic processes [20]. Figure 3 shows an example of OEO phase noise. The loop noise is  $S_\psi(f) = 8 \times 10^{-12}/f + 10^{-14}$ , the same used in Subsection 5.F. The periodicity of the delay-line phase produces a series of noise peaks at frequency multiples of  $1/\tau_d$ . These peaks have an

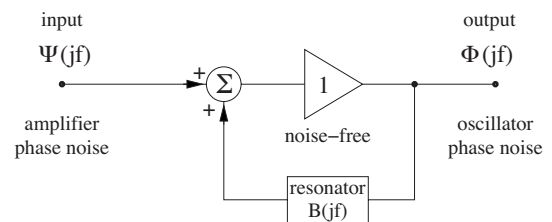


Fig. 2. Oscillator phase-noise model.

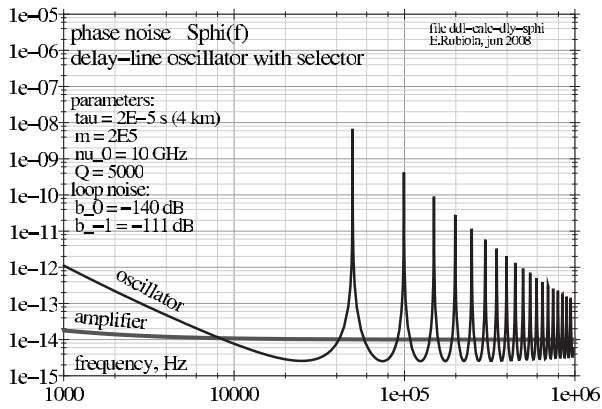


Fig. 3. Calculated OEO phase noise.

extremely narrow bandwidth, in the hertz range, but in simulations and experiments they seem significantly wider because of the insufficient resolution. The peak height follows the law  $S_{\phi}(f) \sim 1/f^4$  (-40 dB/decade). Eliyahu and Maleki [[21] Section 4] report about a discrepancy by a factor of  $\sqrt{f}$  (-35 dB/decade), yet giving little detail and suggesting that further investigation is necessary.

### 3. OPTICAL-FIBER MICROWAVE DELAY

#### A. Design Strategy

The optical-fiber delay unit, shown in Fig. 4, is designed for low noise and high stability of the delay, as discussed below. Focusing on the X band, for practical reasons we chose standard 7–12.4 GHz microwave components, mainly intended for radar and telecommunication technology.

The optical fiber is a Corning SMF-28 wound on a cylinder of 15 cm diameter and 2 cm height. We used 2 km (10  $\mu$ s) and 4 km (20  $\mu$ s) fibers in most experiments; sometimes we used shorter ones. The spool is enclosed in a 5 mm thick Duralumin cylinder thermally insulated from the environment by a 3 cm plastic foam layer. The cylinder is stabilized at room temperature within a fraction of a millikelvin with a proportional-integral-derivative (PID) control built in our laboratory, and set with the Ziegler–Nichols method. The ultimate period, i.e., the inverse oscillation frequency of the proportional-only control at the oscillation threshold, is of 40 s. The advantage of the control versus a passive stabilization (large metal mass and insulator) is still questionable. In the short term the passive stabilization would certainly be preferable because it does not suffer from the noise inher-

ent in the control. On the other hand, in phase-noise measurements (Fig. 5) we need to stabilize the quadrature condition at the mixer inputs during the session, which lasts up to one day. Moreover, in dual-channel measurements (Section 4) the residual environment fluctuations are fully correlated, while the thermal fluctuations of the control can be rejected because the two controls are independent.

The light source is a semiconductor Cable TV laser, temperature controlled and powered with a low-noise current source. This choice is partially motivated by the need for reasonable simplicity and low relative intensity noise (RIN). The RIN turns into AM noise of the detected microwave signal, which pollutes the phase-noise measurements (Subsection 4.A). During the past two years we used both 1.31 and 1.55  $\mu$ m lasers. The fiber attenuation is of 0.2 dB/km at 1.55  $\mu$ m, and of 0.35 dB/km at 1.31  $\mu$ m. The dispersion of the SMF-28 fiber goes to zero at  $1.311 \pm 0.01 \mu$ m, which virtually eliminates the effect of the laser frequency noise in the vicinity of that wavelength. For reference, at 1.55  $\mu$ m the dispersion is of 17 (ps/nm)/km. A laser linewidth of 10 MHz ( $5.8 \times 10^{-5}$  nm) at 1.55  $\mu$ m produces a delay fluctuation of  $2 \times 10^{-15}$  s rms after 2 km optical fiber, which is equivalent to  $1.2 \times 10^{-4}$  rad at the microwave frequency of 10 GHz. The frequency flicker of one of our lasers, measured in the frequency domain with an asymmetric Mach–Zehnder and converted into Allan deviation  $\sigma_y(\tau)$ , is of  $4 \times 10^{-10}$ . This preliminary result indicates that the laser fluctuation should be less than 100 kHz (flicker floor), which gives a phase-noise contribution lower than other noises. In the end, we have a weak preference for the 1.55  $\mu$ m lasers, based on the more progressed technology, and after comparing empirically the effect of several lasers on the phase-noise spectra.

The intensity modulator is a Mach–Zehnder electro-optic modulator (EOM) exhibiting low half-wave voltage ( $V_{\pi} \approx 3.9$  V), so that the maximum modulation is achieved with no more than 50 mW (+17 dBm) of microwave power. This choice is important for the stability of the bias point because the LiNbO<sub>3</sub> is highly sensitive to temperature, thus to power and thermal gradients. Other modulation methods have been discarded: the direct modulation of the laser because the laser threshold enhances the microwave phase noise, and the acousto-optic modulator because it is unsuitable to microwaves.

For low noise the photodetector can only be a InGaAs p-i-n diode operated in strong reverse-bias conditions, thus operated as a photoconductor. Reverse bias is necessary for high speed, as it reduces the capacitance. The need for low noise excludes some other detectors, such as the avalanche diode. The traditional photodetectors loaded to a resistor are preferred to the more modern ones with an internal transconductance amplifier because of the possibility to choose a low-flicker external amplifier.

#### B. Output Power and White Noise

Using the subscript  $\lambda$  for light and the overbar for the time average, the modulated optical power at the output of the EOM is

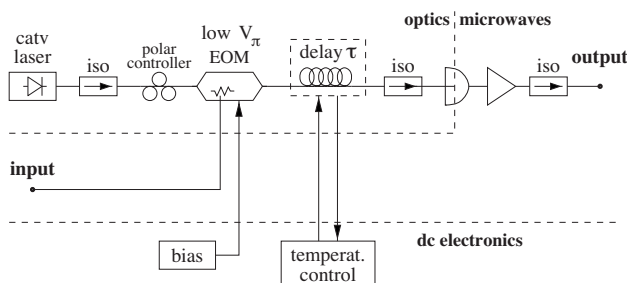


Fig. 4. Optical-fiber delay unit.

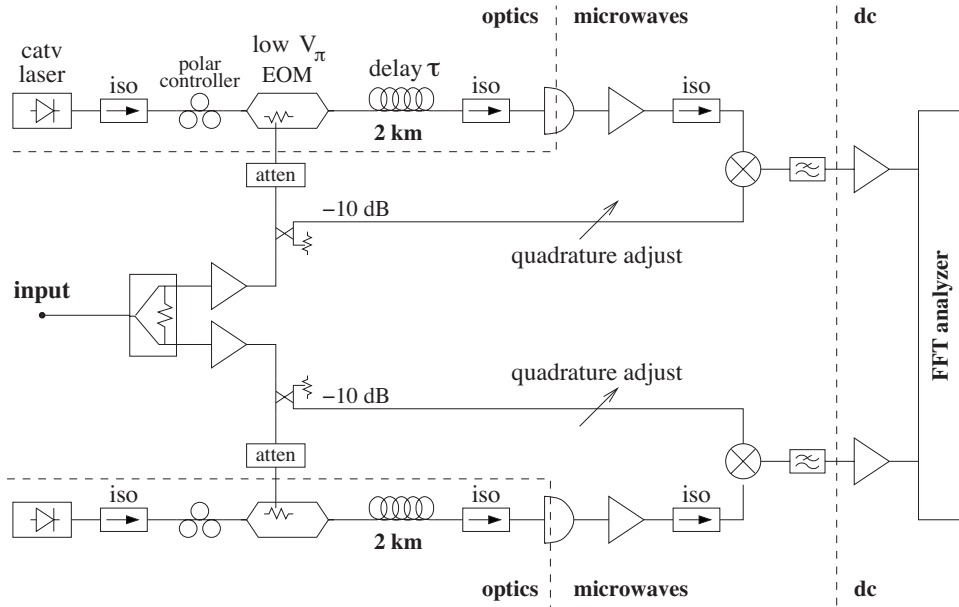


Fig. 5. Scheme of the dual-channel instrument.

$$P_\lambda(t) = \bar{P}_\lambda[1 + m_i \cos(2\pi\nu_0 t)], \quad (18)$$

where the intensity-modulation index is

$$m_i = 2J_1\left(\frac{\pi V_p}{V_\pi}\right), \quad (19)$$

where  $J_1(\cdot)$  is the first-order Bessel function,  $V_p$  is the microwave peak voltage, and  $V_\pi$  is the modulator half-wave voltage. Equation (19) originates from the sinusoidal nature of the EOM response, with  $V_p \cos(2\pi\nu_0 t)$  input voltage. The harmonics at frequency  $n\nu_0$ , integer  $n \geq 2$ , fall beyond the microwave bandwidth, thus they are discarded. Though the maximum modulation index is  $m_i = 1.164$ , occurring at  $V_p = 0.586V_\pi$ , the practical values are 0.8–1.

The detected photocurrent is  $i(t) = \rho P_\lambda(t)$ , where  $\rho$  is the detector responsivity. Assuming a quantum efficiency of 0.6, the responsivity is of 0.75 A/W at 1.55  $\mu\text{m}$  wavelength, and of 0.64 A/W at 1.31  $\mu\text{m}$ . The dc component of  $i(t)$  is  $i_{dc} = \rho \bar{P}_\lambda$ . The microwave power at the detector output is

$$P_0 = \frac{1}{2} m_i^2 R_0 \rho^2 \bar{P}_\lambda^2 \quad (\text{detector output}), \quad (20)$$

where  $R_0 = 50 \Omega$  is the load resistance.

The white noise at the input of the amplifier is

$$N = FkT_0 + 2qR_0\rho\bar{P}_\lambda \quad (\text{white noise}), \quad (21)$$

where  $F$  is the amplifier noise figure and  $kT_0 = 4 \times 10^{-21}$  J is the thermal energy at room temperature. The first term of Eq. (21) is the noise of the amplifier, and the second term is the shot noise. Using  $b_0 = N/P_0$ , the white phase noise is

$$b_0 = \frac{2}{m_i^2} \left[ \frac{FkT_0}{R_0} \frac{1}{\rho^2 \bar{P}_\lambda^2} + \frac{2q}{\rho \bar{P}_\lambda} \right] \quad (\text{white phase noise}). \quad (22)$$

Interestingly, the noise floor is proportional to  $1/\bar{P}_\lambda^2$  at low power, and to  $1/\bar{P}_\lambda$  above the threshold power

$$P_\lambda = \frac{FkT_0}{R_0} \frac{1}{2\rho q} \quad (\text{threshold power}). \quad (23)$$

For example, taking  $\rho = 0.75$  A/W and  $F = 5$  (SiGe parallel amplifier), we get a threshold of 1.7 mW, at which the noise floor is  $b_0 \approx 10^{-15}$  rad<sup>2</sup>/Hz (−150 dBrad<sup>2</sup>/Hz).

### C. Flicker Noise

Phase and amplitude flickering result from the near-dc 1/f noise upconverted by nonlinearity or by a parametric modulation process. This is made evident by two simple facts:

1. The 1/f noise is always always present in the dc bias of electronic devices.
2. In the absence of a carrier, the microwave spectrum at the output of a device is white, i.e., nearly constant in a wide frequency range.

Assuming that the phase modulation is approximately linear unless the carrier is strong enough to affect the dc bias, two basic rules hold:

1.  $b_{-1}$  is independent of the carrier power.
2. Cascading two or more devices the  $b_{-1}$  add up, regardless of the device order in the chain.

The reader may have in mind the Friis formula for the noise referred to as the input of a chain [22], stating that the contribution of each stage is divided by the total gain of the preceding stages, and therefore indicating the first stage as the major noise source. The Friis formula arises

from the additive property of white noise, hence it does not apply to parametric noise.

Early measurements on amplifiers [23–25] suggest that different amplifiers based on a given technology tend to have about the same  $b_{-1}$ , and that  $b_{-1}$  is nearly constant in a wide range of carrier frequency and power. Our independent experiments confirm that the  $1/f$  phase noise of a given amplifier is independent of power in a wide range [[26,27,19] (Chap. 2)]. For example,  $b_{-1}$  of a commercial amplifier (Microwave Solutions MSH6545502) that we measured at 9.9 GHz is between  $1.25 \times 10^{-11}$  and  $2 \times 10^{-11}$  from 300 to 80 mW of output power. Similarly, the  $1/f$  noise of a LNPT32 SiGe amplifier measured between 32  $\mu$ W (–15 dBm) and 1 mW (0 dBm) in 5 dB steps overlap perfectly. In summary, the typical phase flickering  $b_{-1}$  of a “good” microwave amplifier is between  $10^{-10}$  and  $10^{-12}$  rad<sup>2</sup>/Hz (–100 to –120 dBrad<sup>2</sup>/Hz) for the GaAs HBTs, and between  $10^{-12}$  and  $10^{-13}$  rad<sup>2</sup>/Hz (–120 to –130 dBrad<sup>2</sup>/Hz) for the SiGe transistors.

The  $1/f$  noise of the microwave photodetector is expected to be similar to that of an amplifier because the underlying physics and technology are similar. The measurement is a challenging experimental problem, which has been tackled only at the NASA–Caltech Jet Propulsion Laboratory (JPL) (Pasadena, Calif.) independently by Shieh *et al.*, [28], Shieh and Maleki [29], and Rubiola *et al.* [30]. The results agree in that at 10 GHz the typical  $b_{-1}$  of an InGaAs p-i-n photodetector is of  $10^{-12}$  rad<sup>2</sup>/Hz (–120 dBrad<sup>2</sup>/Hz).

Microwave variable attenuators and variable phase shifters can be necessary for adjustment. Our early measurements [31] indicate that the  $b_{-1}$  of these components is of the order of  $10^{-15}$  rad<sup>2</sup>/Hz (–150 dBrad<sup>2</sup>/Hz), which is negligible as compared to the amplifiers and to the photodetectors.

Additional sources of noise are the EOM, the laser amplified spontaneous emission, and the noise of the optical pump. As theory provides no indications about these effects, a pragmatic approach is necessary, which consists of measuring the total noise of the microwave delay unit in different configurations.

#### 4. DUAL-DELAY PHASE NOISE MEASUREMENT

Figure 5 shows the scheme of the instrument. However similar it is to the previous ones ([12,32]), this version adds engineering and substantial progress in understanding  $1/f$  noise. The instrument consists of two equal and independent channels that measure the oscillator under test using the principle of Fig. 1. Then, the single-channel noise is removed using the cross-spectrum method before converting the mixer output into the oscillator noise  $S_{\varphi}(f)$  with Eq. (18).

Looking at one channel, we observe that the microwave signal is split into two branches before the EOM, so that the long branch consists of a modulator, optical fiber (delay  $\tau$ ), a photodetector, and a microwave amplifier, while the short branch is a microwave path of negligible length. This differs from the first single-channel instrument [[10], Fig. 7], in which the short branch was optical. Removing the photodetector and the microwave amplifier from the

short branch yields lower noise, and in turn faster convergence of the correlation algorithm. Lower laser power is needed. Another advantage is that we use a microwave power splitter instead of an optical power splitter. While the noise of the former is negligible for our purposes [33,34], we have no firsthand knowledge about the latter. The problem with this configuration is that we no longer have an optical input, so the microwave-modulated light beams cannot be measured.

Trading off with the available components, we had to use both GaAs amplifiers and SiGe amplifiers. Since the SiGe amplifiers exhibit lower  $1/f$  noise, they are inserted at the photodetector output. This choice is motivated by the fact that the  $1/f$  noise at the mixer input is converted into oscillator  $1/f^{\beta}$  noise by Eqs. (12) and (13) while the  $1/f$  noise at the EOM input is not.

##### A. Mixer Noise

Used as a phase detector, the double-balanced mixer needs to be saturated at both inputs. The conversion gain is of 0.1–0.5 V/rad when the power is in the appropriate range, which is of  $\pm 5$  dB centered around the optimum power of 5–10 mW. Out of this range,  $b_{-1}$  increases. At lower power the conversion gain drops suddenly because the input voltage is insufficient for the internal Schottky diodes to switch.

Out of our experience in low-flicker applications, we have a preference for the mixers manufactured by Narda West (division of L3 Communications Co., New York, USA) and Marki Microwave Inc. (Morgan Hill, CA, USA). The coefficient  $b_{-1}$  is of the order of  $10^{-12}$ , similar to that of the photodetectors. The white noise is chiefly the noise of the output amplifier divided by the conversion gain  $k_{\varphi}$ . Assuming that the amplifier noise is 1.6 nV/ $\sqrt{\text{Hz}}$  (our low-flicker amplifiers input-terminated to 50  $\Omega$  [35]) and that  $k_{\varphi}=0.1$  V/rad (conservative with respect to  $P_0$ ), the white noise is  $b_0=2.5 \times 10^{-16}$  rad<sup>2</sup>/Hz (–156 dBrad<sup>2</sup>/Hz).

Mixers are sensitive to the amplitude noise  $\alpha(t)$  of the input signal, hence the mixer output takes the form  $v(t) = k_{\varphi}\varphi(t) + k_{\alpha}\alpha(t)$ . This is due to the asymmetry of the internal diodes and baluns. In some cases we have measured  $k_{\varphi}/k_{\alpha}$  of 5 or less, while values of 10–20 are common. In photonic systems the contamination from amplitude noise can be a serious problem because of the power of some lasers and laser amplifiers fluctuates. Brendel *et al.* [36] and Cibel *et al.* [37] suggest that the mixer can be operated at a sweet point off the quadrature, where the sensitivity to AM noise nulls. A further study shows that the Brendel offset method cannot be used in our case [38] because the null of amplitude sensitivity results from the equilibrium between equal and opposite sensitivities at the two inputs. But the delay decorrelates the mixer input signals by virtue of the same mechanism used to measure  $S_{\varphi}(f)$ .

##### B. Calibration

The phase-noise measurement system is governed by  $S_v(f) = k_{\varphi}^2 |H(jf)|^2 S_{\varphi}(f)$  [Eqs. (12) and (13)]. Calibration takes the accurate measurement of  $\tau$  and  $k_{\varphi}$ . An accuracy of 1 dB can be expected. Since the stability of the optical fiber exceeds our needs,  $\tau$  does not need recalibration after the initial setup. Optical reflection methods are suit-

able, as well as the spectrum measurement of the noise the peak at  $f=1/\tau$ , where  $|H(jf)|^2=0$ . Conversely,  $k_\varphi$  is highly sensitive to optical and microwave power. It is therefore recommended to measure it at least every time the experimental conditions are changed.

The simplest way to measure  $k_\varphi$  is to introduce a reference sinusoidal modulation  $\varphi(t)=m_\varphi \sin(2\pi f_m t)$  in the microwave signal [Eq. (1)], after replacing the oscillator under test with a microwave synthesizer. This accounts for the dc amplifier at the mixer output, not shown in Fig. 1. It is convenient to set  $f_m \leq 0.1/\tau$ , so that it holds  $\sin(\pi f_m \tau) \approx \pi f_m \tau$  in Eq. (13). With commercial synthesizers frequency modulation is more suitable than phase modulation because the frequency deviation  $\Delta f$  can be measured in static conditions, with dc input. Frequency modulation is equivalent to phase modulation

$$\varphi(t) = \frac{\Delta f}{f_m} \sin 2\pi f_m t, \quad (24)$$

of index  $m_\varphi = \Delta f/f_m$ . Substituting Eq. (24) into Eq. (1) and truncating the series expansion to the first order, the microwave signal is

$$v(t) = J_0\left(\frac{\Delta f}{f_m}\right) \cos 2\pi \nu_0 t + J_1\left(\frac{\Delta f}{f_m}\right) [\cos 2\pi(\nu_0 + f_m)t - \cos 2\pi(\nu_0 - f_m)t], \quad (25)$$

where  $J_n(\cdot)$  is the Bessel function of order  $n$ . For small  $m_\varphi$ , we use the approximations  $J_0(m_\varphi) \approx 1$  and  $J_1(m_\varphi) \approx \frac{1}{2}m_\varphi$ . Thus,

$$v(t) = \cos 2\pi \nu_0 t + \frac{1}{2} \frac{\Delta f}{f_m} [\cos 2\pi(\nu_0 + f_m)t - \cos 2\pi(\nu_0 - f_m)t]. \quad (26)$$

Finally, the modulation index can be easily calibrated by inspection with a microwave spectrum analyzer. In this case it is recommended to measure  $m_\varphi$  with relatively large sidebands (say, 40 dB below the carrier), and then to reduce  $m_\varphi$  by inserting a calibrated attenuator at the FM input of the synthesizer. This enhances the accuracy of the spectrum analyzer. For example, having  $\tau=10 \mu\text{s}$  and  $k_\varphi=0.2 \text{ V/rad}$ , we may set  $f_m=5 \text{ kHz}$  and  $m_\varphi=2 \times 10^{-2} \text{ rad}$ . In this case, the detected signal has a peak voltage of  $400 \mu\text{V}$  at the mixer output, thus 40 mV after 40 dB amplification. Measuring  $k_\varphi$ , it may be convenient to attenuate the modulating signal by 20–30 dB, so that the system is calibrated in actual operating conditions.

## 5. EXPERIMENTS

### A. Measurement of the Background at Zero Fiber Length

Replacing the spools of Fig. 5 with short fibers, the oscillator phase noise is rejected. The noise phenomena originated inside the fiber, or taken in by the fiber, are also eliminated. The noise measured in these conditions (Fig. 6) is the instrument background as it would be with noise-free fibers. Curve a (red) is the phase noise  $S_\varphi(f)$  measured by the mixer output. The other curves (b)–(f) are plotted using the same data set, after inverting  $S_\varphi(f)$

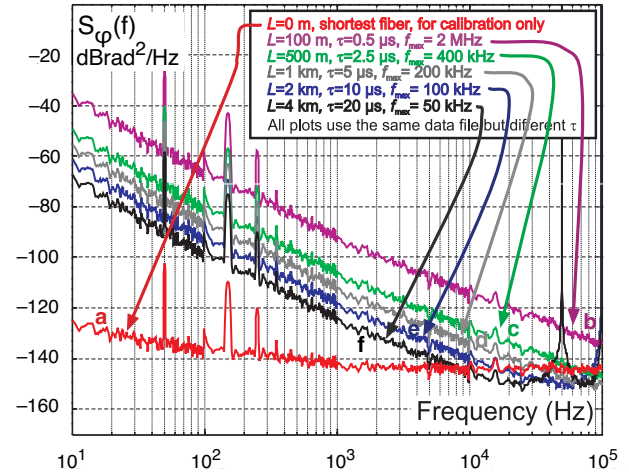


Fig. 6. (Color online) Measured single-channel background noise with zero-length optical fiber.

$=k_\varphi^2 |H(jf)|^2 S_\varphi(f)$  for various fiber lengths [Eqs. (12) and (13)]. As expected after Subsection 2.C, curve f (black, 4 km fiber,  $\tau=20 \mu\text{s}$ ) shows a peak at  $1/\tau=50 \text{ kHz}$  and at  $2/\tau=100 \text{ kHz}$ , due to the division by  $|H(jf)|^2=0$ . Additionally, curve f shows two minima 6 dB lower than  $S_\varphi(f)$  at  $f=25$  and  $75 \text{ kHz}$ , where  $|H(jf)|^2=4$ . The same phenomena are observed at twice the frequency on curve e (blue, 2 km fiber,  $\tau=10 \mu\text{s}$ ), although the 100 kHz peak is hidden by curve f.

### B. Effect of Microwave AM Noise and of Laser Relative Intensity Noise

This experiment shows qualitatively the effect of the laser RIN and the AM noise of the oscillator under test, still in single-channel mode and with zero-length optical fiber, so that the oscillator phase noise is rejected (Fig. 7). Curve 3 (red) is the same as curve a of Fig. 6. In this case, the optical source is a CATV laser, while the oscillator under test is a 10 GHz sapphire-loaded dielectric-cavity oscillator operated at room temperature [11]. Besides high stability, the sapphire oscillator performs low AM noise. Replacing the laser with a different one with higher RIN (curve 2, blue), or replacing the oscillator under test with a synthesizer (curve 3, black), which has higher AM noise, the background increases significantly.

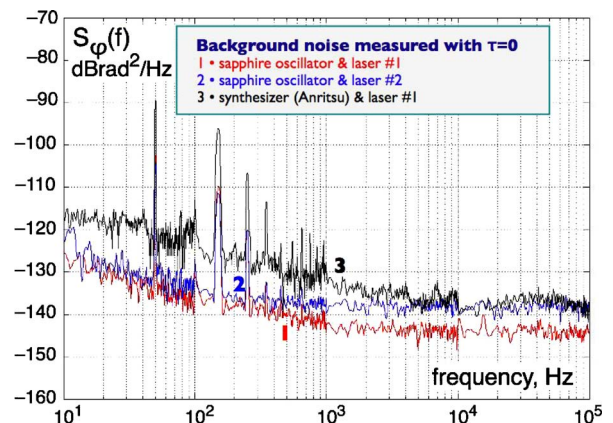


Fig. 7. (Color online) Effect of the laser RIN and the oscillator-under-test AM noise, measured with zero-length fiber.

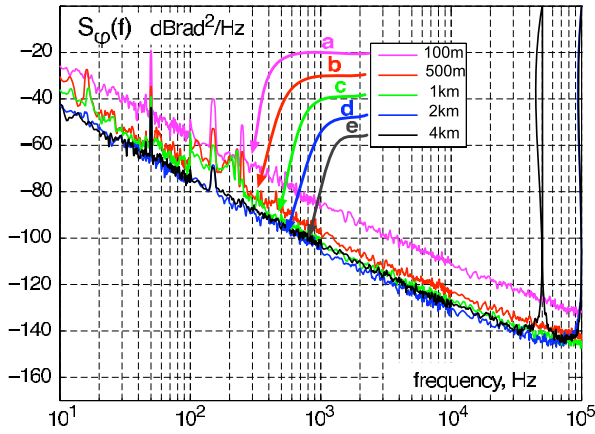


Fig. 8. (Color online) Phase noise of a sapphire oscillator.

### C. Measurement of a Sapphire Microwave Oscillator

We measured the phase noise of a room-temperature sapphire oscillator, still in single-channel mode, progressively increasing the fiber length (Fig. 8). The sharp peak of curve e (black) at  $1/\tau=50$  kHz and  $2/\tau=100$  kHz are due to the division by  $|H(jf)|^2=0$ , as explained in Subsection 2.C. Of course this peak is not present in the oscillator noise. Let us focus on the  $1/f^3$  noise, which dominates on the spectrum. When the delay is insufficient to detect the noise of the source under test, the spectrum is the background of the instrument, which scales with the inverse square length, that is,  $-6$  dB in  $S_\varphi(f)$  for a factor of 2 in the delay. This is visible on curves a (magenta, 100 m,  $\tau=0.5 \mu\text{s}$ ) and b (red, 500 m,  $\tau=2.5 \mu\text{s}$ ). Increasing the length, the  $1/f^3$  noise no longer decreases. This fact, seen on curves d (blue, 2 km,  $\tau=10 \mu\text{s}$ ) and e (black, 4 km,  $\tau=20 \mu\text{s}$ ), indicates that the instrument measures the phase noise of the sapphire oscillator, which does not scale with the delay. Measuring the  $1/f^3$  noise of a sapphire oscillator in single-channel mode is a remarkable result because this oscillator is regarded as the best reference in the field of low-noise microwave sources.

### D. Assessing the Noise of the Photonic Channel

We measured the phase noise of the photonic channel using the scheme of Fig. 9, derived from Fig. 5 after removing some parts. The phase noise of the reference oscillator is rejected by using two fibers of equal length. This experiment suffers from the following limitations.

1. The noise of the fibers cannot be separated from other noises.
2. The  $1/f$  noise of the GaAs amplifiers that drive the EOM can show up.
3. We could not use the correlation method because it takes four matched optical delay lines, which were not available.

Nonetheless, this scheme has the merit of giving at least an upper bound of the achievable noise. The measured spectrum, shown in Fig. 10, indicates that the  $1/f$  phase noise is  $b_{-1}=8 \times 10^{-12}$  rad<sup>2</sup>/Hz ( $-111$  rad<sup>2</sup>/Hz). At this level, the mixer noise is negligible.

### E. Background Noise of the Two-Channel Instrument

We measured the background noise in the two-channel configuration, using the cross-spectrum method of Subsection 2.B and with zero-length optical fiber, so that the phase noise of the 10 GHz reference oscillator is rejected. This experiment does not account for the optical noises originating inside the fibers; these phenomena are rejected in Eq. (13) because the two fibers cannot be correlated. When this experiment was done, the stability of the quadrature condition was still insufficient for long acquisitions. For this reason we stopped the measurement after  $m=200$  spectra. The cross spectrum is shown in Fig. 11.

The reference straight line (red) is the  $1/f^3$  phase noise equivalent to the Allan deviation  $\sigma_y=10^{-12}$ , calculated with Eqs. (4) and (5). Thus, averaging on 200 spectra the instrument can measure the stability of an oscillator at the  $10^{-12}$  level.

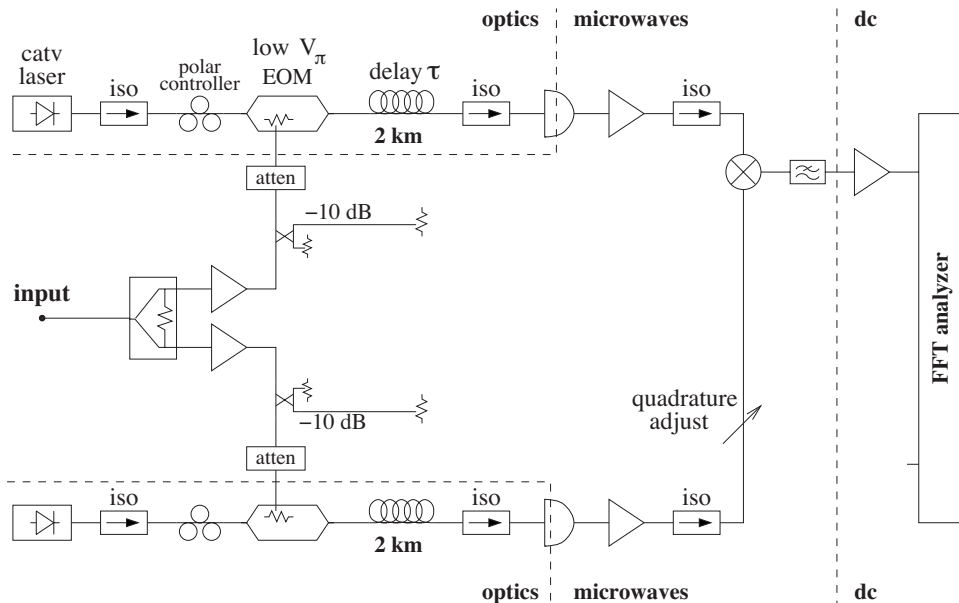


Fig. 9. Measurement of the background noise, including the optical fibers.

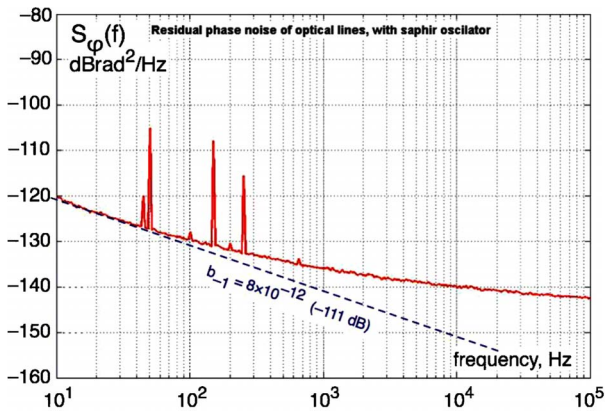


Fig. 10. (Color online) Background noise, including the optical fibers.

The signature of a correlated noise is a smooth cross spectrum. Yet, in Fig. 11 the variance is far too large for the two channels to be correlated. This indicates that the sensitivity is limited by the small number of averaged spectra. Additionally, the spectrum shows a sawtoothlike discrepancy versus the  $1/f^3$  line. This averaging effect, due to the measurement bandwidth that increases with frequency in logarithmic resolution, further indicates that the value of  $m$  is still insufficient. The ultimate sensitivity for large  $m$  is still not known.

**F. Opto-Electronic Oscillator**

We implemented the oscillator of Fig. 12 using a 4 km delay line (20  $\mu$ s), a SiGe amplifier, and a photodetector with an integrated transconductance amplifier. Oscillation starts at 6–7 mW optical power. The best working point occurs at 12–13 mW optical power, where the microwave output power is 20 mW. For flicker noise the microwave chain is similar to one channel in Fig. 9 because the order of the devices in the chain is not relevant. Thus, we take  $b_{-1} = 8 \times 10^{-12}$  rad<sup>2</sup>/Hz (–111 dBrad<sup>2</sup>/Hz), the same as that of Fig. 10, as the first estimate of the loop noise. Though somewhat arbitrary, this value accounts for the photodetector internal amplifier, more noisy than our microwave amplifiers. Using  $(b_{-1})_{loop} = 8 \times 10^{-12}$  rad<sup>2</sup>/Hz in the oscillator noise model of Subsection 2.D, the expected oscillator flickering is  $(b_{-3})_{osc} = 6.3 \times 10^{-4}$  rad<sup>2</sup>/Hz

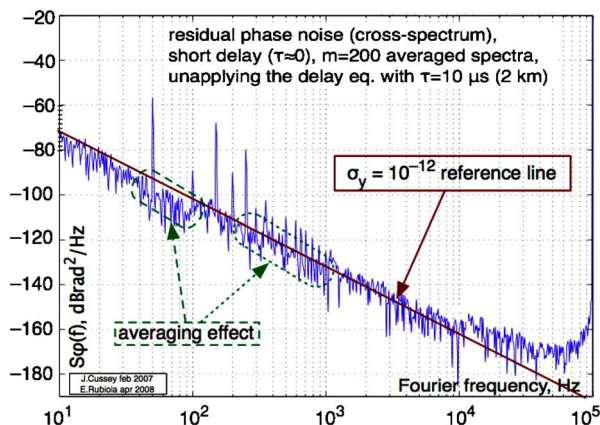


Fig. 11. (Color online) Background noise in two-channel mode, measured with zero-length fiber.

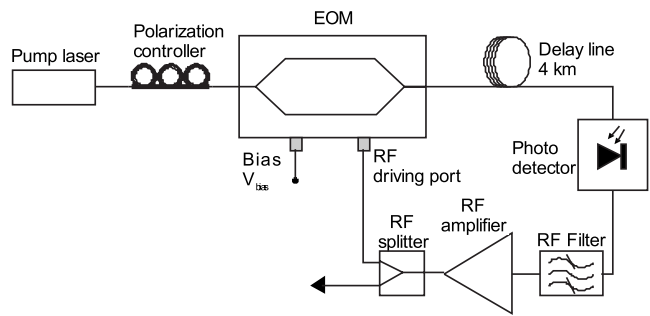


Fig. 12. Scheme of the optoelectronic oscillator.

(–32 dBrad<sup>2</sup>/Hz). By virtue of Eq. (4) and (5), this is equivalent to a frequency stability  $\sigma_y = 2.9 \times 10^{-12}$  (Allan deviation). The noise spectrum (Fig. 13), measured with the dual-channel instrument, shows a frequency flicker of  $10^{-3}$  rad<sup>2</sup>/Hz (–30 dBrad<sup>2</sup>/Hz), equivalent to  $\sigma_y = 3.6 \times 10^{-12}$ . The discrepancy between the predicted value and the result is 2 dB.

Interestingly, the OEO phase noise compares favorably to the lowest-noise microwave synthesizers and quartz oscillator multiplied to 10 GHz. Yet, the OEO can be switched in steps of 50 kHz without degrading the noise.

**6. FURTHER DEVELOPMENTS**

Our experiments suggest the following improvements, tested or in progress.

1. In the phase-noise instrument, the microwave power the input of the EOM and the two inputs of the mixer is a critical parameter because the gain of the entire system is strongly nonlinear. The insertion of test points is recommended, using common and inexpensive power detectors after tapping a fraction of the power with 20 dB directional couplers.
2. The instrument requires that the two signals at the mixer input are kept in quadrature. This is usually accomplished with a line stretcher or a with voltage-controlled phase shifter. A smarter solution exploits the dispersion of the optical fiber by adjusting the laser wavelength via the temperature control [39]. This is viable

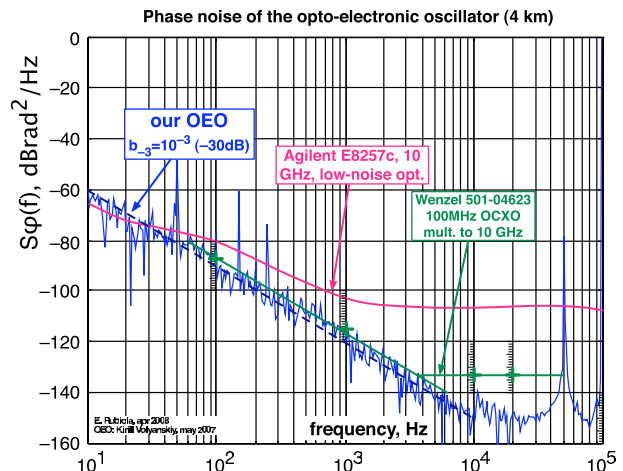


Fig. 13. (Color online) Phase noise of the optoelectronic oscillator.

only at  $1.55\ \mu\text{m}$  and with long fibers. For reference, using a 2 km fiber and our lasers, it takes 10 K of temperature change for a quarter wavelength of the microwave signal. Another solution exploits the temperature coefficient of the fiber delay,  $6.85 \times 10^{-6}/\text{K}$ . Accordingly, a quarter wavelength takes 0.37 K of temperature with 2 km fiber ( $10\ \mu\text{s}$ ), or 3.7 K with 200 m.

3. Some popular EOMs have a low-frequency photodetector at the unused output port of the Mach–Zehnder interferometer, which we hope to exploit to stabilize the bias point.

4. The OEO frequency can be fine-tuned by adding a RF signal with an SSB modulator at the output. Extremely high resolution, of the order of  $10^{-16}$ , can be obtained with a 48 bit DDS, with no degradation of the spectral purity [40,41].

## ACKNOWLEDGMENTS

We are indebted to Lute Maleki [OEwaves and NASA–Caltech (JPL), Pasadena, Calif., USA], Nan Yu (NASA/Caltech JPL) and Ertan Salik (NASA–Caltech JPL, now with the California State Polytechnic University, Pomona, Calif., USA) for having taught us a lot in this domain, and for numerous discussions, advice, and exchanges. Gilles Cibiel (Centre National d’Etudes Spatiales (CNES), France) provided contract support and help. Rodolphe Boudot (FEMTO-ST, now with Systèmes de Référence Temps-Espace (SYRTE), Paris, France) helped with the sapphire oscillator, Xavier Jouvenceau (FEMTO-ST) helped in the implementation of the early version of the correlation system, and Cyrus Rocher (FEMTO-ST) implemented the temperature control.

This work is supported with grants from Aeroflex, CNES, and Agence Nationale de la Recherche (ANR).

## REFERENCES

- W. S. C. Chang, ed., *RF Photonic Technology in Optical Fiber Links* (Cambridge U. Press 2002).
- T. A. Yilmaz, C. M. Depriest, A. Braun, J. Abeles, and P. J. Delfyett, “Noise in fundamental and harmonic modelocked semiconductor lasers: experiments and simulations,” *IEEE J. Quantum Electron.* **39**, 838–849 (2003).
- D. J. Jones, K. W. Holman, M. Notcutt, J. Ye, J. Chandalia, L. A. Jiang, E. P. Ippen, and H. Yokoyama, “Ultralow-jitter, 1550-nm mode-locked semiconductor laser synchronized to a visible optical frequency standard,” *Opt. Lett.* **28**, 813–815 (2003).
- X. S. Yao and L. Maleki, “Optoelectronic microwave oscillator,” *J. Opt. Soc. Am. B* **13**, 1725–1735 (1996).
- X. S. Yao, L. Davis, and L. Maleki, “Coupled optoelectronic oscillators for generating both RF signal and optical pulses,” *J. Lightwave Technol.* **18**, 73–78 (2000).
- K. J. Vahala, “Optical microcavities,” *Nature* **424**, 839–846 (2003).
- T. J. Kippenberg, S. M. Spillane, and K. J. Vahala, “Kerr-nonlinear optical parametric oscillation in an ultrahigh-Q toroid microcavity,” *Phys. Rev. Lett.* **93**, 083904 (2004).
- A. A. Savchenkov, A. B. Matsko, D. Strekalov, M. Mohageg, V. S. Ilchenko, and L. Maleki, “Low threshold optical oscillations in a whispering gallery mode  $\text{CaF}_2$  resonator,” *Phys. Rev. Lett.* **93**, 1–4 (2004).
- S. T. Cundiff and J. Ye, “Colloquium: femtosecond optical frequency combs,” *Rev. Mod. Phys.* **75**, 325–342 (2003).
- E. Rubiola, E. Salik, S. Huang, and L. Maleki, “Photonic delay technique for phase noise measurement of microwave oscillators,” *J. Opt. Soc. Am. B* **22**, 987–997 (2005).
- V. Giordano, P.-Y. Bourgeois, Y. Gruson, N. Boubekeur, R. Boudot, E. Rubiola, N. Bazin, and Y. Kersalé, “New advances in ultra-stable microwave oscillators,” *Eur. Phys. J.: Appl. Phys.* **32**, 133–141 (2005).
- E. Salik, N. Yu, L. Maleki, and E. Rubiola, “Dual photonic-delay-line cross correlation method for the measurement of microwave oscillator phase noise,” in *Proceedings of the European Frequency Time Forum and Frequency Control Symposium Joint Meeting* (2004), pp. 303–306.
- J. Rutman, “Characterization of phase and frequency instabilities in precision frequency sources: fifteen years of progress,” *Proc. IEEE* **66**, 1048–1075 (1978).
- H. G. Kimball, ed., *Handbook of Selection and Use of Precise Frequency and Time Systems* (ITU, 1997).
- CCIR Study Group VII, *Characterization of Frequency and Phase Noise*, Report No. 580-3, in *Standard Frequencies and Time Signals*, Vol. VII (annex) of Recommendations and Reports of the CCIR (International Telecommunication Union, 1990), pp. 160–171.
- J. R. Vig (chair.), *IEEE Standard Definitions of Physical Quantities for Fundamental Frequency and Time Metrology-Random Instabilities IEEE Standard 1139-1999* (IEEE, 1999).
- J. Vanier and C. Audoin, *The Quantum Physics of Atomic Frequency Standards* (Hilger, 1989).
- E. Rubiola, “The Leeson effect,” arXiv:physics/0502143v1, web site arxiv.org (2005). Abridged draft version of [19].
- E. Rubiola, *Phase Noise and Frequency Stability in Oscillators* (Cambridge U. Press, 2008).
- Y. K. Chembo, K. Volyanskiy, L. Larger, E. Rubiola, and P. Colet, “Determination of phase noise spectra in optoelectronic microwave oscillators: a phase diffusion approach,” *J. Quantum Electron.* (to be published).
- D. Elyahu and L. Maleki, “Low phase noise and spurious level in multi-loop opto-electronic oscillators,” in *Proceedings of the European Frequency Time Forum and Frequency Control Symposium Joint Meeting* (2003), pp. 405–410.
- H. T. Friis, “Noise figure of radio receivers,” *Proc. IRE* **32**, 419–422 (1944).
- D. Halford, A. E. Wainwright, and J. A. Barnes, “Flicker noise of phase in RF amplifiers: characterization, cause, and cure,” (Abstract) in *Proceedings of Frequency Control Symposium* (1968), pp. 340–341.
- F. L. Walls, E. S. Ferre-Pikal, and S. R. Jefferts, “Origin of  $1/f$  PM and AM noise in bipolar junction transistor amplifiers,” *IEEE Trans. Ultrason. Ferroelectr. Freq. Control* **44**, 326–334 (1997).
- A. Hati, D. Howe, D. Walker, and F. Walls, “Noise figure vs. PM noise measurements: a study at microwave frequencies,” in *Proceedings of the European Frequency Time Forum and Frequency Control Symposium Joint Meeting* (2003).
- E. Rubiola and R. Boudot, “ $1/f$  noise of RF and microwave amplifiers,” available soon on <http://arxiv.org>.
- R. Boudot, “Oscillateurs micro-onde à haute pureté spectrale,” Ph.D. dissertation (Université de Franche Comté, 2006).
- W. Shieh, X. S. Yao, L. Maleki, and G. Lutes, “Phase-noise characterization of optoelectronic components by carrier suppression techniques,” in *Proceedings of the Optical Fiber Communication (OFC) Conference* (1998), pp. 263–264.
- W. Shieh and L. Maleki, “Phase noise characterization by carrier suppression techniques in RF photonic systems,” *IEEE Photon. Technol. Lett.* **17**, 474–476 (2005).
- E. Rubiola, E. Salik, N. Yu, and L. Maleki, “Flicker noise in high-speed p-i-n photodiodes,” *IEEE Trans. Microwave Theory Tech.* **54**, 816–820 (2006).
- E. Rubiola, V. Giordano, and J. Gros Lambert, “Very high

- frequency and microwave interferometric PM and AM noise measurements," *Rev. Sci. Instrum.* **70**, 220–225 (1999).
32. P. Salzenstein, J. Cussey, X. Jouvenceau, H. Tavernier, L. Larger, E. Rubiola, and G. Sauvage, "Realization of a phase noise measurement bench using cross correlation and double optical delay line," *Acta Phys. Pol. A* **112**, 1107–1111 (2007).
  33. E. Rubiola and V. Giordano, "Correlation-based phase noise measurements," *Rev. Sci. Instrum.* **71**, 3085–3091 (2000).
  34. E. Rubiola and V. Giordano, "Advanced interferometric phase and amplitude noise measurements," *Rev. Sci. Instrum.* **73**, 2445–2457 (2002).
  35. E. Rubiola and F. Lardet-Vieudrin, "Low flicker-noise amplifier for 50  $\Omega$  sources," *Rev. Sci. Instrum.* **75**, 1323–1326 (2004).
  36. R. Brendel, G. Marianneau, and J. Ubersfeld, "Phase and amplitude modulation effects in a phase detector using an incorrectly balanced mixer," *IEEE Trans. Instrum. Meas.* **26**, 98–102 (1977).
  37. G. Cibiel, M. Régis, E. Tournier, and O. Llopis, "AM noise impact on low level phase noise measurements," *IEEE Trans. Ultrason. Ferroelectr. Freq. Control* **49**, 784–788 (2002).
  38. E. Rubiola and R. Boudot, "The effect of AM noise on correlation phase noise measurements," *IEEE Trans. Ultrason. Ferroelectr. Freq. Control* **54**, 926–932 (2007).
  39. K. Volyanskiy and L. Larger, *Quadrature Stabilization in the Opto-Electronic Phase-Noise Measurement System by Laser Tuning*, FEMTO-ST internal report (FEMTO-ST, 2008), personal communication.
  40. *Elisa—Technical Notes of the ESA Cryo Project*, Series of FEMTO-ST and ESA internal reports (FEMTO-ST, 2007–2008).
  41. "Analog devices AD9854 DDS," <http://www.analog.com/>.